INTERNATIONAL JOURNAL FOR NUMERICAL METHODS IN ENGINEERING, VOL. 37, 2445–2470 (1994)

A THREE-DIMENSIONAL LAYER-WISE CONSTANT SHEAR ELEMENT FOR GENERAL ANISOTROPIC SHELL-TYPE STRUCTURES

RAFFAELE ZINNO

Department of Structural Engineering, University of Calabria, 87030 Arcavacata di Rende (Cosenza), Italy

EVER J. BARBERO

Department of Mechanical and Aerospace Engineering, West Virginia University, Morgantown, WV 26506, U.S.A.

SUMMARY

This paper deals with the development of a new three-dimensional element with two-dimensional kinematic constraints capable of analysing the mechanical behaviour of the laminated anisotropic shell-type structures. This element, originally developed for the linear analysis of plates, is extended for the linear analysis of laminated composite shells. The element can represent arbitrarily curved shells with variable number of layers and thicknesses, including ply drop-off problems. The element was validated in a previous work by the patch test. All the analytical details necessary to make possible the shell analysis are presented here. Examples are reported to show the capability of the element to predict the behaviour of complex structures and a refined computation of the stresses is carried out by integrating the equilibrium equations.

1. INTRODUCTION

Thin and thick shells are popular and useful forms of structural components with many applications in engineering. Particularly, in weight sensitive applications, where high strength-to-weight ratios are needed, the advent of new types of composite materials, makes appropriate the use of multilayered composite shells. This has led to great interest in the development of adequate theories for modelling the behaviour of the general anisotropic shell-type structures.

The solution of such laminated composites having complex geometry, arbitrary loading and boundary conditions, presents intractable analytical problems and the finite element formulation provides a convenient method of solution. The classical Love thin shell theory is based on the Kirchhoff hypotheses. It assumes the laminae to be in the state of plane stress and neglects the transverse shears and normal strain in the thickness direction. Ambartsumyan[1] developed a laminated composite shell theory assuming that the individual lamina is orthotropic and oriented in such a way that the principal axes of material symmetry coincide with the principal co-ordinate of the shell reference surface. Dong and Taylor[2] presented an extension of Donnel's shallow shell theory to thin laminated shells in which, as in the Kirchhoff–Love theory, the transverse shear deformation is neglected.

The effects of transverse shear deformation and the magnitude of the errors, inherent to the basic Kirchhoff–Love theory assumptions are discussed by Koiter.[3] In fact as the shell becomes thicker, compared to its radii of curvature and in-plane dimensions, the transverse effects become more pronounced. These effects are very important in the case of laminated composite shells

CCC 0029–5981/94/142445–26$9.00

Received 1 July 1993
Revised 10 November 1993

because of their low transverse shear moduli compared to their longitudinal moduli. For this reason, in recent years, attempts have been made to do away with one or more of Kirchhoff's foregoing assumptions. Reddy[4] applied the First-order Shear Deformation Theory (FSDT) to both single and doubly curved anisotropic shells. Reddy and Chandrashekara[5] solved both cylindrical and spherical laminated shell cases accounting for transverse shear deformation, while Bruno *et al.*[6] studied the non-linear behaviour of thick doubly curved composite shells made in *unimodular* and *bimodular* materials. In the FSDT, constant shear rotation is assumed through the shell thickness. This requires the use of a shear correction coefficient whose accurate prediction for an anisotropic laminated shell is cumbersome and problem dependent.

To obtain an improvement in the determination of the stress distribution through the thickness, overcoming the use of the shear correction coefficient and satisfying the traction-free boundary conditions, higher-order theories have been presented. In particular the third-order theories are capable of representing a quadratic shear distribution through the thickness of a homogeneous shell. All third-order theories can be derived from a common set of kinematical assumptions.[7] In general, single-layer laminate theories, especially the FSDT are adequate in representing global behaviour (e.g. deflections, fundamental frequencies, etc.) but inadequate in accurately representing local effects, such as interlaminar stress distribution, delaminations, etc. All single-layer theories are based on one displacement expansion throughout the thickness of the laminate. Consequently, the transverse strains are continuous through the laminate thickness. Such theories cannot accurately model laminates made of dissimilar material layers because as a result of the different material properties, the out-of-plane stress components are discontinuous at the interfaces between layers, thus violating the equilibrium conditions. Noting this restriction of the traditional plate and shell theories, several authors[8–17] proposed Layer-wise Constant Shear Theories (LCST). In these theories the distribution of the displacements is continuous through the thickness of the shell with derivatives with respect to the thickness coordinate that are not necessarily continuous at the interfaces between layers. The finite element implementation of these theories is not simple because they imply a large number of degrees of freedom (d.o.f) per node. Moreover, the physical interpretation of the d.o.f and the large number of the stress resultants and displacements is not as intuitive as in the single layer theories. Two-dimensional LCST have not been used for shells because of the complexity of the formulation except for the case of cylindrical shells.[10]

A three-dimensional shell element based on the application of two-dimensional kinematic constraints of the FSDT to a continuum element was developed by Ahmad *et al.*[18] for the analysis of thick and thin shell structures. They noted that the retention of three degrees of freedom at each node leads to large stiffness coefficients for relative displacements along an edge corresponding to the shell thickness. This presents numerical problems and inevitably leads to ill-conditioned equations when the shell thicknesses become small compared with the other dimensions of the element. The second factor showed by Ahmad *et al.*[18] is that of economy. The use of several nodes across the shell thickness ignores the well known fact that even for thick shells the *normals* to the middle surface remain practically straight after deformation. Thus an unnecessarily high number of d.o.f has to be carried, involving penalties of computer time.

In previous works Barbero[19,20] developed a new element for the analysis of laminated plates starting from the formulation of Ahmad *et al.*,[18] and substituting the assumption of the normals to the middle surface straight after deformation with the assumptions of the LCST. In particular he noted that with the use of a 3-D element, it is possible to analyse laminated composite shells overcoming the difficulties linked with the LCST but retaining the precise stress calculation. Barbero and Zinno[21] completed the work in References 19 and 20 developing a procedure for the refined calculation of the interlaminar stresses along the lines of previous work[22,23] and validating by the patch-test the 3-Dimensional Layer-wise Constant Shear (3DLCS) element.

However, all the computations in References 19–21 were performed for plate problems. Several extension and modifications of the work presented in References 19–21 are presented here to make the analysis of the general shell-type structures possible. First, a surface co-ordinate system is defined. Next, the kinematics of References 19–21 is modified to allow for the correct evaluation of the element strain matrix, taking into account the membrane effect. Finally, a procedure for the refined computations of the shell's interlaminar stresses is developed. The procedure requires computations of higher-order derivatives of the shape functions. These derivatives are presented here in the context of the isoparametric formulation of three-dimensional problems.

To overcome the problem shown by Ahmad *et al.*[18] of the unnecessarily high number of d.o.f, when the 3-D continuum elements are utilized in the analysis of composite laminated structures, the formulation takes into account the assumption of the incompressibility along the thickness direction. This assumption is quite valid for a broad class of problems of moderately thick laminates. A method is presented that by applying a particular constraint matrix takes into account the incompressibility of the normals to the middle surface and reduces the number of global d.o.f. Thus the proposed element has a small number of d.o.f per node and produces results as accurate as conventional 3-D continuum elements for a large range of problems.

With this element the imposition of the boundary condition, loads, etc., has a very simple physical interpretation. It is also possible to model problems with variable number of layers (ply drop-off) and variable thickness because the position of the middle surface is irrelevant. Some examples are presented to show the capability of the proposed element to produce results as accurate as 3-D continuum elements overcoming the problems of the ill-conditioned equations.

2. FORMULATION OF THE PROBLEM

With reference to Figure 1, a general laminated composite shell with n unidirectionally fibre-reinforced homogeneous orthotropic layers is examined. The orthotropic axes of symmetry in each lamina of arbitrary thickness and elastic properties are oriented at an arbitrary angle with respect to the surface axes defined in Section 3. The total thickness of the shell is h. Each point of the shell is defined by its co-ordinate x, y, z with respect to a global system of reference. A displacement-based finite element procedure is employed for the numerical solution in the context of the total Lagrangian formulation.

Let $\{\mathbf{u}\} = \{u, v, w\}^{\mathrm{T}}$ the displacement of each point of the shell. The equilibrium of the structure occupying a volume V with boundary ∂V, is represented by the virtual work expression:

$$\int_V \{\mathbf{d}\boldsymbol{\varepsilon}\}^{\mathrm{T}}\{\boldsymbol{\sigma}\}\,\mathrm{d}V = \int_V \{\mathbf{du}\}^{\mathrm{T}}\{\mathbf{p}\}\,\mathrm{d}V + \int_{\partial V} \{\mathbf{du}\}^{\mathrm{T}}\{\mathbf{q}\}\,\mathrm{d}A \qquad (1)$$

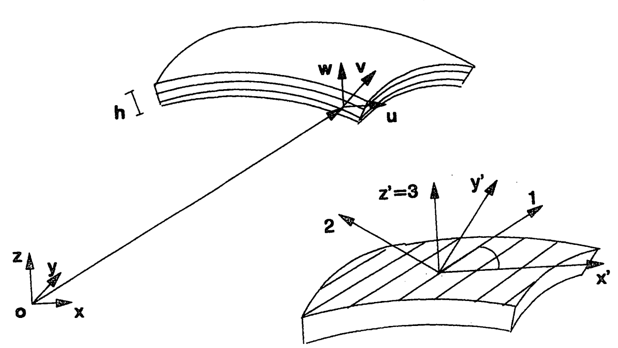

Figure 1. Shell geometry

where $\{\mathbf{du}\}$ are the virtual displacements, $\{\boldsymbol{\sigma}\}$ is the symmetric Cauchy stress tensor, and $\{\boldsymbol{\varepsilon}\}$ is the linear infinitesimal strain tensor associated with the displacements $\{\mathbf{u}\}$.

The Cauchy stress tensor components and the infinitesimal strain tensor are related, for the kth lamina, through the constitutive tensor components $\bar{C}^k_{ijrs}$. The constitutive matrix can be written with respect to the material directions (1, 2, 3) as

$$[\bar{\mathbf{D}}^k] = \begin{bmatrix} \bar{Q}^k_{11} & \bar{Q}^k_{12} & \bar{C}^k_{13} & 0 & 0 & 0 \\ \bar{Q}^k_{12} & \bar{Q}^k_{22} & \bar{C}^k_{23} & 0 & 0 & 0 \\ \bar{C}^k_{13} & \bar{C}^k_{23} & \bar{C}^k_{33} & 0 & 0 & 0 \\ 0 & 0 & 0 & k^2\bar{C}^k_{44} & 0 & 0 \\ 0 & 0 & 0 & 0 & k^2\bar{C}^k_{55} & 0 \\ 0 & 0 & 0 & 0 & 0 & \bar{Q}^k_{66} \end{bmatrix} \tag{2}$$

Because of the transverse incompressibility assumption ($\bar{\varepsilon}^k_{33} = 0$) used in the kinematics, the inplane components of the constitutive matrix must be replaced by the plane stress reduced stiffness coefficients $\bar{Q}_{ij}$,[24] while the out of plane coefficients $\bar{C}_{ij}$ are obtained from the three-dimensional elasticity tensor.[25] The shear correction coefficient k is included as required by FSDT ($k^2 = 5/6$). The need to use a shear correction factor reduces as the number of the elements through the thickness of the laminate increases. This can be easily explained for the case of an isotropic shell as follows. An assemblage of 3DLCS elements through the thickness represents the parabolic distribution of the shear stress by a layer-wise constant approximation. As the number of layers increases the error reduces and no shear correction factor is needed. Using this expression for $[\bar{\mathbf{D}}]$ and setting $\bar{\varepsilon}^k_{33} = 0$, we can overcome large stiffness coefficients for relative displacements along an edge corresponding to the shell thickness and then overcome the numerical problem that can produce ill-conditioned equations when the shell thickness becomes small compared to the other dimensions in the element.

The constraint that normals remain perpendicular to the middle surface has been deliberately omitted to account for shear deformations. Moreover, if we use one element for each lamina (or cluster of laminae) we omit the constraint that the normals remain straight after deformation, obtaining the Layer-wise Constant Shear model where the rotations of each lamina are independent.

Using the rotation matrix

$$[\mathbf{T}^k] = \begin{bmatrix} \cos^2\vartheta^k & \sin^2\vartheta^k & 0 & 0 & 0 & 2\sin\vartheta^k\cos\vartheta^k \\ \sin^2\vartheta^k & \cos^2\vartheta^k & 0 & 0 & 0 & -2\sin\vartheta^k\cos\vartheta^k \\ 0 & 0 & 1 & 0 & 0 & 0 \\ 0 & 0 & 0 & \cos\vartheta^k & -\sin\vartheta^k & 0 \\ 0 & 0 & 0 & \sin\vartheta^k & \cos\vartheta^k & 0 \\ -\sin\vartheta^k\cos\vartheta^k & \sin\vartheta^k\cos\vartheta^k & 0 & 0 & 0 & \cos^2\vartheta^k - \sin^2\vartheta^k \end{bmatrix} \tag{3}$$

we can obtain the expression of $[\mathbf{D}^k]$ written with respect to the surface system of reference

$$[\mathbf{D}^k] = [\mathbf{T}^k]^{-1}[\bar{\mathbf{D}}^k][\mathbf{T}^k] \tag{4}$$

Thus the relationship between stresses and strains with reference to the surface co-ordinate system and taking into account that the index k can be deleted because each lamina k is here considered modelled by one or more 3DLCS elements

$$\{\boldsymbol{\sigma}'\} = [\mathbf{D}]\{\boldsymbol{\varepsilon}'\} \tag{5}$$

At every point of the shell surface we can erect a normal z' with two orthogonal axes x' and y' tangent to it on this surface (Figure 1). It must be noted that in general none of these directions coincide with those of the curvilinear co-ordinates of the element (ξ, η, ζ) (see Section 3), although x', y' are in the $\xi-\eta$ plane (ζ = constant). Here and in the following, comma indicates a derivative with respect to the indicated co-ordinate.

The strains components of interest are

$$\{\boldsymbol{\varepsilon}'\} = \left\{\begin{matrix} \varepsilon'_{x'} \\ \varepsilon'_{y'} \\ 0 \\ \gamma'_{y'z'} \\ \gamma'_{x'z'} \\ \gamma'_{x'y'} \end{matrix}\right\} = \left\{\begin{matrix} u'_{,x'} \\ v'_{,y'} \\ 0 \\ w'_{,y'} + v'_{,z'} \\ w'_{,x'} + u'_{,z'} \\ u'_{,y'} + v'_{,x'} \end{matrix}\right\} \tag{6}$$

with the strain in direction z' neglected so as to be consistent with the shell LCST assumption of incompressibility of normals. In fact, for a large range of problems we can assume that the elongation of segments normal to the middle surface is zero during the deformation.

3. FINITE ELEMENT DEVELOPMENT

The displacement $\{\mathbf{u}\} = \{u, v, w\}^{\mathrm{T}}$ inside an element can be written as $\{\mathbf{u}\} = [\mathbf{N}]\{\boldsymbol{\delta}\}$, where $\{\boldsymbol{\delta}\}$ is the collection of the nodal $\{\boldsymbol{\delta}_i\}$ that in this formulation is $\{\boldsymbol{\delta}_i\} = \{u_i, v_i, w_i\}^{\mathrm{T}}$. The interpolation functions are equal for u, v and w:

$$\left\{\begin{matrix} u \\ v \\ w \end{matrix}\right\} = \sum_{k=1}^{\mathcal{N}} \begin{bmatrix} N_i & 0 & 0 \\ 0 & N_i & 0 \\ 0 & 0 & N_i \end{bmatrix} \{\boldsymbol{\delta}_i\} \tag{7}$$

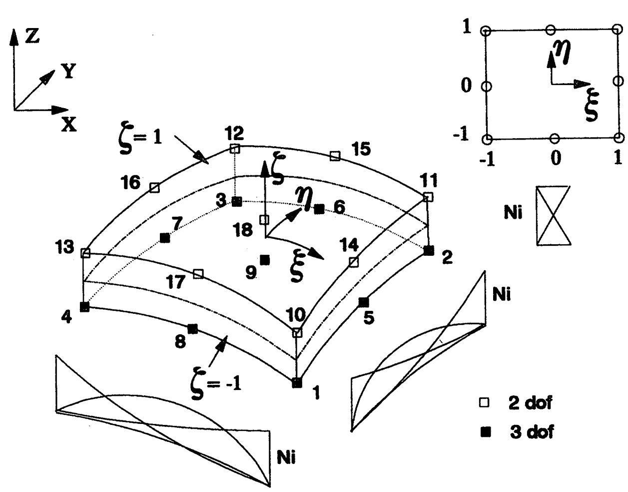

Figure 2. The 3DLCS element

where $\mathcal{N}$ is the number of the nodes and $N_i = N_i(\xi, \eta, \zeta)$. The order of interpolation functions N_i along the two directions on the surface of the shell can be chosen independently of the order through the thickness. Linear or quadratic interpolation of the displacements (u, v) are commonly used. The order of approximation in the thickness direction for the displacement w corresponds to different kinematical assumptions in LCST. A linear variation is used in this paper, but higher-order approximation functions can be easily implemented (Figure 2).

The linear variation through the thickness of the element presents several advantages:

(a) It reproduces FSDT kinematic assumption when a single element is used to model the entire thickness of the laminate.
(b) It reproduces LCST kinematic constraints when the element is used to model a single layer of laminate. It was demonstrated by comparison with exact solutions that the layer-wise linear distribution is the most efficient one.[9] Therefore, more refined approximations through the thickness (e.g. quadratic, cubic spline) are not usually necessary. However, they can be easily implemented.
(c) The computational cost is reduced with respect to three-dimensional quadratic finite elements (20 or 27 node brick elements).

In this paper, the resulting element satisfies the incompressibility condition of normals to the middle surface of FSDT and other theories. Furthermore, the computational cost is significantly reduced since all nodes through the thickness have the same transverse deflection which can be represented as a single degree of freedom for each location on the surface of the shell.

Using the equations (5) and (1) where the term on the left-hand side is the strain energy and the terms on the right-hand side are the work of the body forces and distributed surface loads, we can obtain

$$\int_V [\mathbf{B}']^{\mathrm{T}}\{\boldsymbol{\sigma}\}\,\mathrm{d}V = \int_V [\mathbf{N}]^{\mathrm{T}}\{\mathbf{p}\}\,\mathrm{d}V + \int_{\partial V} [\mathbf{N}]^{\mathrm{T}}\{\mathbf{q}\}\,\mathrm{d}A \tag{8}$$

where $[\mathbf{B}']$ is the strain–displacement matrix connecting the strains $\{\boldsymbol{\varepsilon}'\}$, written with respect to the surface co-ordinates, to the nodal displacement vector, written with respect to the global co-ordinate system of reference, as described in equation (10). It is necessary to use the $[\mathbf{B}']$ matrix instead of

$$[\mathbf{B}] = \begin{bmatrix} N_{i,x} & 0 & 0 \\ 0 & N_{i,y} & 0 \\ 0 & 0 & 0 \\ 0 & N_{i,z} & N_{i,y} \\ N_{i,z} & 0 & N_{i,x} \\ N_{i,y} & N_{i,x} & 0 \end{bmatrix} \tag{9}$$

because the $[\mathbf{D}]$ matrix in equation (4) is written with respect to the surface co-ordinate system.

The equilibrium equations for an element are obtained simply replacing in equation (8) the body volume V by the element volume V_e and the body surface ∂V by the element surface ∂V_e.

Using the kinematic equation

$$\{\boldsymbol{\varepsilon}'\} = [\mathbf{B}']\{\boldsymbol{\delta}\} \tag{10}$$

and the constitutive equation (5) into the equilibrium equation (8) written with respect to an element, we obtain the element stiffness matrix as:

$$[\mathbf{K}^e] = \int_{V_e} [\mathbf{B}']^{\mathrm{T}}[\mathbf{D}][\mathbf{B}']\,\mathrm{d}V_e \tag{11}$$

The derivatives of the displacements with respect to the global axes (x, y, z) are obtained in the standard way as

$$\begin{bmatrix} u_{,x} & v_{,x} & w_{,x} \\ u_{,y} & v_{,y} & w_{,y} \\ u_{,z} & v_{,z} & w_{,z} \end{bmatrix} = [\mathbf{J}]^{-1} \begin{bmatrix} u_{,\xi} & v_{,\xi} & w_{,\xi} \\ u_{,\eta} & v_{,\eta} & w_{,\eta} \\ u_{,\zeta} & v_{,\zeta} & w_{,\zeta} \end{bmatrix} \tag{12}$$

where the Jacobian matrix is calculated from the co-ordinate definition.[21] Now, for every set of curvilinear co-ordinates, the global displacement derivatives can be obtained numerically. A further transformation to surface directions (x', y', z') will allow the strain, and hence the $[\mathbf{B}']$ matrix, to be evaluated.

First the directions of the surface axes have to be established. The scheme adopted in the present work for the choice of the surface x'- or y'-axis is advantageous for the analysis of fibre-reinforced composites because it facilitates the specification of the fibre-orientation on each lamina. A vector normal to the surface ζ = constant can be bound as a vector product of any two vectors tangent to the surface (Figure 3),

$$\{\mathbf{V}_3\} = \begin{Bmatrix} x_{,\xi} \\ y_{,\xi} \\ z_{,\xi} \end{Bmatrix} \times \begin{Bmatrix} x_{,\eta} \\ y_{,\eta} \\ z_{,\eta} \end{Bmatrix} = \begin{Bmatrix} y_{,\xi} z_{,\eta} - y_{,\eta} z_{,\xi} \\ x_{,\eta} z_{,\xi} - x_{,\xi} z_{,\eta} \\ x_{,\xi} y_{,\eta} - x_{,\eta} y_{,\xi} \end{Bmatrix} \tag{13}$$

When the vector $\{\mathbf{V}_3\}$ is defined, it is possible to erect an infinity of mutually perpendicular vectors orthogonal to it. For instance, if $(\mathbf{i}\}$ is the unit vector along the x-axis, we define

$$\{\mathbf{V}_2\} = \{\mathbf{i}\} \times \{\mathbf{V}_3\} \tag{14}$$

which makes the vector $\{\mathbf{V}_2\}$ perpendicular to the plane defined by the direction $\{\mathbf{V}_3\}$ and the x-axis. As $\{\mathbf{V}_1\}$ has to be orthogonal to both $\{\mathbf{V}_3\}$ and $\{\mathbf{V}_2\}$, we have

$$\{\mathbf{V}_1\} = \{\mathbf{V}_3\} \times \{\mathbf{V}_2\} \tag{15}$$

The three directions $\{\mathbf{V}_1\}$, $\{\mathbf{V}_2\}$ and $\{\mathbf{V}_3\}$ are divided by their scalar lengths, giving the unit vectors $\{\mathbf{v}_1\}$, $\{\mathbf{v}_2\}$ and $\{\mathbf{v}_3\}$. If the direction of the x-axis and $\{\mathbf{V}_3\}$ coincide, and this scheme breaks down, the program starts with a unit vector $\{\mathbf{j}\}$ along the y-axis. The unit vectors $\{\mathbf{v}_1\}$, $\{\mathbf{v}_2\}$ and $\{\mathbf{v}_3\}$ define the surface axes (x', y', z'). In particular the scheme adopted to make these vectors is very useful for the analysis of laminated composite shells. In fact, the position of the element in the space is important only for the definition of $\{\mathbf{v}_3\}$, while $\{\mathbf{v}_1\}$ and $\{\mathbf{v}_2\}$ are defined

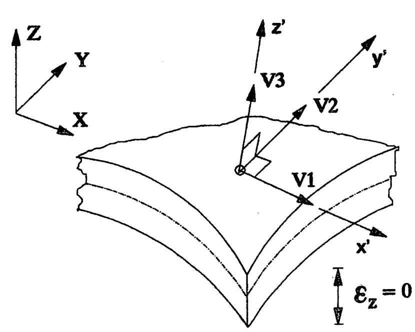

Figure 3. The surface co-ordinate system

with respect to the global x- and y-axes. This is convenient for a simple definition of the fibre orientation angle θ, which can be defined uniquely as the angle between the fibre direction and the x'-axis.

The matrix of unit vectors in directions (x', y', z') is the direction cosine matrix,

$$[\boldsymbol{\Theta}] = [\{\mathbf{v}_1\}, \{\mathbf{v}_2\}, \{\mathbf{v}_3\}] \tag{16}$$

The global derivatives of the displacements u, v and w are now transformed to the surface derivatives of the surface orthogonal displacements by a standard operation

$$\begin{bmatrix} u'_{,x'} & v'_{,x'} & w'_{,x'} \\ u'_{,y'} & v'_{,y'} & w'_{,y'} \\ u'_{,z'} & v'_{,z'} & w'_{,z'} \end{bmatrix} = [\boldsymbol{\Theta}]^{\mathrm{T}} \begin{bmatrix} u_{,x} & v_{,x} & w_{,x} \\ u_{,y} & v_{,y} & w_{,y} \\ u_{,z} & v_{,z} & w_{,z} \end{bmatrix} [\boldsymbol{\Theta}] \tag{17}$$

From this expression, the components of the $[\mathbf{B}']$ matrix can be found explicitly:

$$\{\boldsymbol{\varepsilon}'\} = [\mathbf{B}'] \begin{Bmatrix} \{\boldsymbol{\delta}_1\} \\ \{\boldsymbol{\delta}_2\} \\ \vdots \\ \{\boldsymbol{\delta}_j\} \end{Bmatrix}, \quad \{\boldsymbol{\delta}_i\} = \begin{Bmatrix} u_i \\ v_i \\ w_i \end{Bmatrix} \tag{18}$$

The matrix $[\mathbf{B}']$ is written with respect to the global co-ordinate system and must multiply the global displacements to obtain the strains $[\boldsymbol{\varepsilon}']$ written with respect to the surface co-ordinate system.

In order to evaluate the $[\mathbf{B}']$ matrix the following scheme was employed. Let $[\mathbf{H}]$ be the operator of differentials defined as follows:

$$[\mathbf{H}] = \left[\begin{array}{ccc} \frac{\partial}{\partial x} & 0 & 0 \\ \frac{\partial}{\partial x} & 0 & 0 \\ \frac{\partial}{\partial x} & 0 & 0 \\ \hline 0 & \frac{\partial}{\partial y} & 0 \\ 0 & \frac{\partial}{\partial y} & 0 \\ 0 & \frac{\partial}{\partial y} & 0 \\ \hline 0 & 0 & \frac{\partial}{\partial z} \\ 0 & 0 & \frac{\partial}{\partial z} \\ 0 & 0 & \frac{\partial}{\partial z} \end{array}\right] \tag{19}$$

The linear strains (including ε_{33}) can be expressed as

$$\{\boldsymbol{\varepsilon}\} = [\mathbf{A}][\mathbf{H}][\mathbf{N}]\{\boldsymbol{\delta}\} \tag{20}$$

where

$$[\mathbf{A}] = \begin{bmatrix} 1 & 0 & 0 & 0 & 0 & 0 & 0 & 0 & 0 \\ 0 & 0 & 0 & 0 & 1 & 0 & 0 & 0 & 0 \\ 0 & 0 & 0 & 0 & 0 & 0 & 0 & 0 & 1 \\ 0 & 0 & 0 & 0 & 0 & 1 & 0 & 1 & 0 \\ 0 & 0 & 1 & 0 & 0 & 0 & 1 & 0 & 0 \\ 0 & 1 & 0 & 1 & 0 & 0 & 0 & 0 & 0 \end{bmatrix} \tag{21}$$

Thus, the matrix $[\mathbf{B}]$ can be written as

$$[\mathbf{B}] = [\mathbf{A}][\mathbf{H}][\mathbf{N}] \tag{22}$$

To obtain $[\mathbf{B}']$ we have to rotate $[\boldsymbol{\varepsilon}]$ into $[\boldsymbol{\varepsilon}']$ by using equation (17), but $[\mathbf{B}']$ must multiply $\{\boldsymbol{\delta}\} = \{u_i, v_i, w_i\}^{\mathrm{T}}$, then it is necessary to divide the terms connected with each displacement to take into account the membrane effects of the shells.

Dividing $[\mathbf{H}]$ into three parts as displayed in equation (19) and multiplying $[\mathbf{H}]$ and $[\mathbf{N}]$ we can obtain three matrices. The first matrix is connected only with the u displacements, the second with the v displacements, and the third with the w displacements. Thus, making the operation (17) for each of these matrices we can obtain other three matrices $[\mathbf{a}]$, $[\mathbf{b}]$ and $[\mathbf{c}]$. In these matrices, for example the terms a_{11}, b_{11} and c_{11} are connected with $\partial u'/\partial x'$ in $\{\boldsymbol{\varepsilon}'\}$ but a_{11} must multiply the u-displacements, b_{11} the v-displacements, and the c_{11} the w-displacements. Using these three matrices we can obtain $[\mathbf{B}']$ as follows:

$$[\mathbf{B}']\{\boldsymbol{\delta}\} = \begin{bmatrix} a_{11} & b_{11} & c_{11} & \cdots \\ a_{22} & b_{22} & c_{22} & \cdots \\ 0 & 0 & 0 & \cdots \\ a_{23}+a_{32} & b_{23}+b_{32} & c_{23}+c_{32} & \cdots \\ a_{13}+a_{31} & b_{13}+b_{31} & c_{13}+c_{31} & \cdots \\ a_{12}+a_{21} & b_{12}+b_{21} & c_{12}+c_{21} & \cdots \end{bmatrix} \begin{Bmatrix} u_1 \\ v_1 \\ w_1 \\ \vdots \\ u_n \\ v_n \\ w_n \end{Bmatrix} \tag{23}$$

The terms a_{33}, b_{33} and c_{33} are replaced by zeros due to the incompressibility conditions.

The numerical integration is performed by Gaussian quadrature. A two-point rule suffices in the ζ direction, while a minimum of three or four points in both ξ and η directions is needed for parabolic or cubic elements respectively. Reduced integration is used in the ξ and η directions for the shear terms.

4. ASSEMBLY PROCEDURE AND APPLICATION OF THE CONSTRAINTS

The integration of the element stiffness matrix is performed as a standard 18 nodes element with three degrees of freedom per node (u, v, w) but with the appropriate shape functions N_i previously described.

The surface transverse deflection w' is constant through the thickness of the shell by the incompressibility assumption made omitting ε'_{33} in equation (23). Therefore, we must impose that for two nodes aligned through the thickness we have only one w' (in the bottom for example). If this is not done the stiffness matrix will present a singularity and the solution cannot be reached.

With reference to Figure 4, where three 3DLCS elements are assembled to form a laminate, we have that:

$$w'_1 = w'_2 = w'_3 = w'_4$$

For example we can analyse element number 3 in Figure 4 where we have that the two w'-displacements of element 3 (w'_3, w'_4) must be equal to the displacement w'_1 at the bottom node of element number 1, called *master node*:

$$w'_3 = w'_4 = w'_1$$

Using the direction cosine matrix we can write

$$\{\mathbf{u}'_i\} = [\mathbf{\Theta}^i]^{\mathrm{T}}\{\mathbf{u}_i\} \tag{24}$$

or explicitly

$$\begin{Bmatrix} u'_i \\ v'_i \\ w'_i \end{Bmatrix} = \begin{bmatrix} \Theta^i_{11} & \Theta^i_{21} & \Theta^i_{31} \\ \Theta^i_{12} & \Theta^i_{22} & \Theta^i_{32} \\ \Theta^i_{13} & \Theta^i_{23} & \Theta^i_{33} \end{bmatrix} \begin{Bmatrix} u_i \\ v_i \\ w_i \end{Bmatrix} \tag{25}$$

Using this expression we can write the following constraint matrix (for the example of the third element in the mesh):

$$\begin{Bmatrix} u_3 \\ v_3 \\ w_3 \end{Bmatrix} = \begin{bmatrix} 1 & 0 & 0 & 0 & 0 \\ 0 & 1 & 0 & 0 & 0 \\ \dfrac{-\Theta^3_{13}}{\Theta^3_{33}} & \dfrac{-\Theta^3_{23}}{\Theta^3_{33}} & \dfrac{\Theta^1_{13}}{\Theta^3_{33}} & \dfrac{\Theta^1_{23}}{\Theta^3_{33}} & \dfrac{\Theta^1_{33}}{\Theta^3_{33}} \end{bmatrix} \begin{Bmatrix} u_3 \\ v_3 \\ u_1 \\ v_1 \\ w_1 \end{Bmatrix} \tag{26}$$

This expression can be written for all the 18 nodes in the element, connecting each of them to the

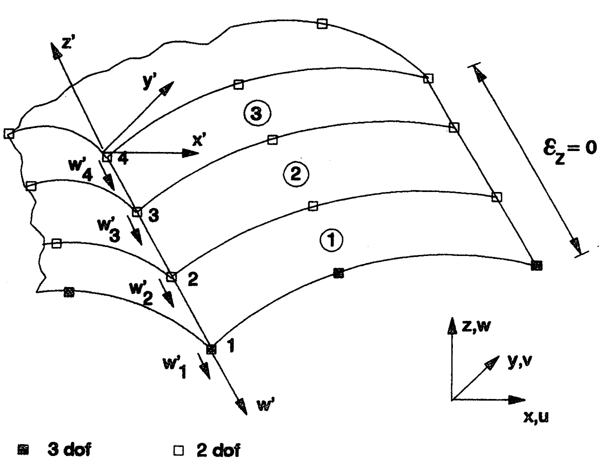

Figure 4. Scheme of an assembly of 3DLCS elements

master node on its vertical, obtaining a constraint matrix [A] of dimensions 54×63. Out of the initial 54 (18×3) d.o.f per element, 36 d.o.f (18×2) corresponding to (u, v) remain independent of the master nodes. The 18 w-d.o.f depend of the $27 (9 \times 3)$ d.o.f (u, v and w) of the master node. They also depend of the 36 d.o.f (u, v) of their own element. Thus we have 63 independent d.o.f $(36 + 27 = 63)$.

The 54×54 standard stiffness matrix (18 nodes with 3 d.o.f) can be written with respect to the independent displacements u and v of all the 18 nodes of the element and u, v and w of the master nodes at the bottom of the shell as follows:

$$[\mathbf{K}^e]_{(63,63)} = [\mathbf{A}]^{\mathrm{T}}_{(63,54)} \, [\mathbf{K}^e]_{(54,54)} \, [\mathbf{A}]_{(54,63)} \tag{27}$$

The nodes at the bottom of the shells are called *master nodes*. However, they can be any set of nodes located at one of the interfaces of the laminate. The location of the *master nodes* through the thickness of the laminate does not affect the results.

The condensation of the redundant degrees of freedom has been easily achieved through the usual assembly by assigning the same global node number of the *master node* to all the w-components of the nodes located on its normal and adding to this node all the contributions of the element stiffness matrix connected to the global displacements of the *master nodes* at the bottom of the shell.

At the end of this condensation we have three degrees of freedom (u, v, w) at the nodes located on the bottom of the structure and only two degrees of freedom (u, v) for all the other nodes in the discretization. Thus we can make a strong reduction of the global degrees of freedom and we can reach a symmetric, banded, non-singular global stiffness matrix.

The displacement w in all the nodes with two degrees of freedom can be easily obtained after the solution, using the equation (26). It is possible to show that for the case of the plate analysis, where the global w are equal on each vertical, that the application of the constraint matrix [A] produces a stiffness matrix of dimensions 45×45. In this case the constraint matrix [A] connects only the global w-displacements of all the nodes with the w-displacements in the bottom of the same vertical. In fact, for the plate analysis the u, v displacements of the master node are not required as described in References 19–21. In this way [A] has a dimension 54×45. Then, during the assemblage we can give the same global node to all the w-nodes through each vertical, so eliminating the singularity of the global stiffness matrix.

The technique adopted has the following advantages:

(a) It eliminates the need for complex bookkeeping to identify individual sets of elements stacked to form a laminate.
(b) It eliminates the need for elements with large number of d.o.f that otherwise result if the assembly through the thickness is performed *a priori*. This is particularly useful for the implementation in commercial FEA codes.[26]

The loads can be defined in surface co-ordinate or in global co-ordinate system. If they are defined in surface co-ordinate system, a rotation is necessary to transform them to global co-ordinates using the full rotation matrix (54×54):

$$\{\mathbf{F}'\} = [\boldsymbol{\Theta}]\{\mathbf{F}\} \tag{28}$$

If a pressure is applied, the calculation of the loaded area in surface co-ordinate is necessary and the nodal forces can be obtained by the knowledge of the Jacobian and the element thickness, using the following relation:

$$\{\mathbb{R}\} = \int_A [\mathbf{N}] \begin{Bmatrix} P_{x'} \\ P_{y'} \\ P_{z'} \end{Bmatrix} \mathrm{d}A = \sum_{r=1}^{\mathrm{ngp}} \sum_{s=1}^{\mathrm{ngp}} \begin{Bmatrix} N_i P_{x'} \\ N_i P_{y'} \\ N_i P_{z'} \end{Bmatrix} W_{\xi r} W_{\eta s} \| J \|_{\xi r \eta s} \frac{2}{T_H} \tag{29}$$

where P_i is the component of the distributed load in the direction i; A is the area of upper, middle or bottom surface of the 3DLCS element, depending on the position of the loading; T_H is the thickness of the 3DLCS element of each Gaussian point (ngp = number of Gaussian points); W is the weight at each Gaussian point; and ζ is equal to 1 or -1 or 0, respectively, when the distributed loading is on upper, bottom or middle surface. When the nodal forces are calculated, the previous relation (28) can be adopted.

5. COMPUTATION OF STRESSES

The constitutive equation (5) is used to obtain all components of stress at the reduced Gauss points. The distribution of in-plane stresses $\sigma_{x'}$, $\sigma_{y'}$ and $\sigma_{x'y'}$ is linear through the thickness. The distribution of inter-laminar stresses $\sigma_{x'z'}$ and $\sigma_{y'z'}$ is layer-wise constant. All components of stress obtained at the integration points can be extrapolated to the nodes using the procedure described by Cook.[27] This is done to facilitate the graphic output using pre- and post-processing package.[28]

Selective reduced integration is used on the shear-related terms. The 3DLCS element reduces to FSDT when only one element is used through the thickness. Therefore, the behaviour of the 9-node Lagrangian FSDT element with selective reduced integration, free of shear locking, is also present in the proposed element when several 3DLCS elements are stacked through the thickness. Furthermore, Barbero and Reddy[22] successfully used selective reduced integration on their LCST element that has the same kinematic as a stack of 3DLCS elements. As shown by Averil,[29] the 9-node Lagrangian element with selective reduced integration does not exhibit locking as the plate (or, in this paper, layer) becomes very thin. This is a remarkable advantage of 3DLCS elements over conventional 3-D continuum elements with full integration.

The 3DLCS element gives a very good representation of all the stress components except σ'_z without the aspect ratio limitations of conventional 3-D continuum elements. When transverse stress σ'_z is needed, either conventional 3-D continuum elements can be used or further post-processing can be done by using the third equilibrium equation:

$$\frac{\partial \sigma'_{x'z'}}{\partial x'} + \frac{\partial \sigma'_{y'z'}}{\partial y'} + \frac{\partial \sigma'_{z'z'}}{\partial z'} + p'_z = 0 \tag{30}$$

Quadratic interlaminar stresses that satisfy the shear boundary conditions at the top and at bottom surfaces of the plate are obtained in this work for arbitrarily curved shell laminated modelled with isoparametric elements. An approximation of the shear stress distribution through each layer with a quadratic function requires $3n$ equations for each of the shear stresses ($\sigma'_{x'z'}$, $\sigma'_{y'z'}$), where n is the number of layers. To obtain these $3n$ equations Chaudhuri[23] proposed that n equations be used to satisfy the n average shear stresses on each layer, two equations be used to impose vanishing shear stresses at the surface of the plate (top and bottom), $n-1$ equations to satisfy the continuity of the shear stresses at the interfaces between layers and the remaining $n-1$ equations be used to compute the jump in $\sigma'_{x'z',z'}$ (or $\sigma'_{y'z',z'}$) at each interface.

The average shear stresses ($\sigma'_{x'z'}$, $\sigma'_{y'z'}$) on each layer are computed from the constitutive equations and the displacement field obtained in the FEA.

In this work, the following equilibrium equations

$$\frac{\partial \sigma'_{x'z'}}{\partial z'} = -\left(\frac{\partial \sigma'_{x'x'}}{\partial x'} + \frac{\partial \sigma'_{x'y'}}{\partial y'}\right); \quad \frac{\partial \sigma'_{y'z'}}{\partial z'} = -\left(\frac{\partial \sigma'_{x'y'}}{\partial x'} + \frac{\partial \sigma'_{y'y'}}{\partial y'}\right) \tag{31}$$

are used to compute $\sigma_{x'z',z'}$ and $\sigma_{y'z',z'}$ directly from the FEA approximation for a curved isoparametric shell element in space. The procedure requires computation of second derivatives of the displacements (u', v', w'). In this work, the second derivatives are obtained (Appendix II) from the shape functions used in the isoparametric formulation.

The derivatives of displacements are defined with respect to the global axes (x, y, z) but, for the shell analysis the stresses calculated respect to the surface axes (x', y', z') are needed.
The operator

$$[\nabla\nabla N] = \left\{ \begin{matrix} \dfrac{\partial}{\partial x} \\ \dfrac{\partial}{\partial y} \\ \dfrac{\partial}{\partial z} \end{matrix} \right\} \left\{ \begin{matrix} \dfrac{\partial N}{\partial x} \\ \dfrac{\partial N}{\partial y} \\ \dfrac{\partial N}{\partial z} \end{matrix} \right\} = \begin{bmatrix} \dfrac{\partial^2 N}{\partial x^2} & \dfrac{\partial^2 N}{\partial x \partial y} & \dfrac{\partial^2 N}{\partial x \partial z} \\ \dfrac{\partial^2 N}{\partial y \partial x} & \dfrac{\partial^2 N}{\partial y^2} & \dfrac{\partial^2 N}{\partial y \partial z} \\ \dfrac{\partial^2 N}{\partial z \partial x} & \dfrac{\partial^2 N}{\partial z \partial y} & \dfrac{\partial^2 N}{\partial z^2} \end{bmatrix} \tag{32}$$

contains all the second derivatives that are needed to solve the problem. Then, it is possible to apply the rule of the change of basis at this operator to obtain the second derivatives of the stresses respect to the surface axes:

$$[\nabla\nabla N'] = \begin{bmatrix} \dfrac{\partial^2 N}{\partial x'^2} & \dfrac{\partial^2 N}{\partial x' \partial y'} & \dfrac{\partial^2 N}{\partial x' \partial z'} \\ \dfrac{\partial^2 N}{\partial y' \partial x'} & \dfrac{\partial^2 N}{\partial y'^2} & \dfrac{\partial^2 N}{\partial y' \partial z'} \\ \dfrac{\partial^2 N}{\partial z' \partial x'} & \dfrac{\partial^2 N}{\partial z' \partial y'} & \dfrac{\partial^2 N}{\partial z'^2} \end{bmatrix} = [\mathbf{\Theta}]^{\mathrm{T}} [\nabla\nabla N] [\mathbf{\Theta}] \tag{33}$$

Using equations (5) and (10) we can write

$$\left\{ \begin{matrix} \sigma'^{k}_{x'x',x'} \\ \sigma'^{k}_{y'y',x'} \\ 0 \\ \sigma'^{k}_{y'z',x'} \\ \sigma'^{k}_{x'z',x'} \\ \sigma'^{k}_{x'y',x'} \end{matrix} \right\} = [\overline{\mathbf{D}^k}] \begin{bmatrix} N_{i,x'x'} & 0 & 0 \\ 0 & N_{i,y'x'} & 0 \\ 0 & 0 & 0 \\ 0 & N_{i,z'x'} & N_{i,y'x'} \\ N_{i,z'x'} & 0 & N_{i,x'x'} \\ N_{i,y'x'} & N_{i,x'x'} & 0 \end{bmatrix} \{\mathbf{\delta}\} = [\overline{\mathbf{D}^k}][\mathbf{B}'_{x'}]\{\mathbf{\delta}\} \tag{34}$$

and similarly

$$\left\{ \begin{matrix} \sigma'^{k}_{x'x',y'} \\ \sigma'^{k}_{y'y',y'} \\ 0 \\ \sigma'^{k}_{y'z',y'} \\ \sigma'^{k}_{x'z',y'} \\ \sigma'^{k}_{x'y',y'} \end{matrix} \right\} = [\overline{\mathbf{D}^k}] \begin{bmatrix} N_{i,x'y'} & 0 & 0 \\ 0 & N_{i,y'y'} & 0 \\ 0 & 0 & 0 \\ 0 & N_{i,z'y'} & N_{i,y'y'} \\ N_{i,z'y'} & 0 & N_{i,x'y'} \\ N_{i,y'y'} & N_{i,x'y'} & 0 \end{bmatrix} \{\mathbf{\delta}\} = [\overline{\mathbf{D}^k}][\mathbf{B}'_{y'}]\{\mathbf{\delta}\} \tag{35}$$

where the matrices $[\mathbf{B}'_{x'}]$ and $[\mathbf{B}'_{y'}]$ are used for the computation of the second derivatives of stresses in the same way as the strain–displacement matrix $[\mathbf{B}']$ is used for the computation of stresses. With the second derivatives of stresses, the parabolic shape of $\sigma'_{x'z'}$ and $\sigma'_{y'z'}$ through the thickness respect to the surface axes can be obtained. Then, by the knowledge of the angle

θ between the surface axes and the material directions (1, 2, 3) (Figure 1), it is possible to calculate the stresses in global direction, which are needed to study the failure or damage of laminated composite shells.

6. NUMERICAL RESULTS

In this section the formulation obtained above is used in the linear analysis of ply drop-off beams, rectangular plates and doubly curved shells, to assess the quality of the proposed element and to display the features of the 3DLCS element in the modelling of general composite laminated structures. Table I contain a list of the material properties considered here. Table II contain a list of the boundary conditions considered in this section.

6.1. Beam drop-off example

To show the capability of the proposed element, the example of a beam with or without the ply drop-off,[30] has been analysed here (Figure 5). The ply drop-off is an important problem in the structures made of composite materials. The middle surface is at different location through the thickness in the thick and in the thin part of the beam. Thus, obtaining an exact solution or a finite element solution for these irregular structures is a major problem. The use of the 3DLCS element overcomes the problem because, in comparison to the two-dimensional plate analysis, the position of the middle surface is irrelevant for the use of this element, as for the 3-D continuum elements. We start considering a beam without ply drop-off to check the results obtained using the proposed element making a comparison between the analytical solution and the finite element one. The structure, made in material I (isotropic), is subjected to a unitary load P applied in the transverse direction. The deflection is calculated at two points A and B as shown in Figure 5 together with the dimensions, the labels and the boundary conditions. The Timoshenko beam theory was used to obtain the analytical solution, adding the bending displacements w_b to the

Table I. Material properties

Material I (isotropic)	
	$E = 29\,000$ Ksi; $\nu = 0{\cdot}294$
Material II	
	$E_1 = 19{\cdot}2 \times 10^6$ psi; $E_2 = E_3 = 1{\cdot}56 \times 10^6$ psi; $G_{12} = G_{13} = 0{\cdot}82 \times 10^6$ psi
	$G_{23} = 0{\cdot}523 \times 10^6$ psi; $\nu_{12} = \nu_{13} = 0{\cdot}24$; $\nu_{23} = 0{\cdot}49$
Material III	
	$E_1 = 40$ psi; $E_2 = E_3 = 1{\cdot}0$ psi; $G_{12} = G_{13} = G_{23} = 0{\cdot}5$ psi
	$\nu_{12} = \nu_{13} = \nu_{23} = 0{\cdot}25$

Table II. Boundary conditions

SS
$u = w = 0$ for the sides parallel to the x-axis
$v = w = 0$ for the sides parallel to the y-axis
CC
$u = v = w = 0$ on all the sides

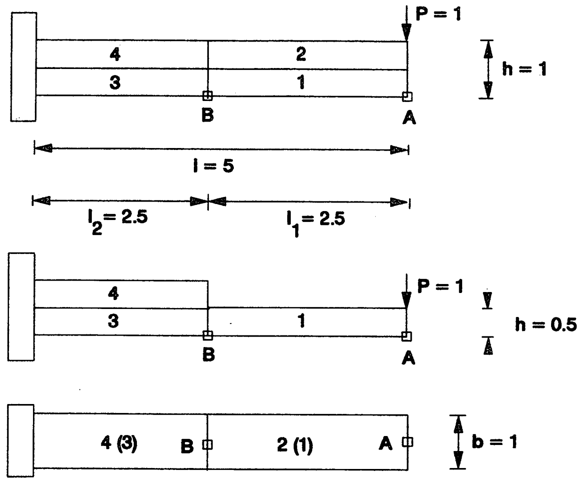

Figure 5. Beam ply drop-off example

shear deflections w_s.

$$\text{point A: } w_t = w_b + w_s = \frac{P\ell^3}{3EI} + \frac{P\ell}{\chi GA} \quad (\chi = 5/6)$$

$$\text{point B: } w_t = w_b + w_s = \frac{5P\ell^3}{48EI} + \frac{P\ell}{2\chi GA}$$

The results obtained using the analytical and the finite element solution are shown in Table III.

To model the ply drop-off beam, one element (number 2) was removed as displayed in the same Figure 5. Referring the thick part by the label 2 and the thin part by the label 1 and using the Timoshenko beam theory we have this expression for the total transverse displacement in the point A:

$$w_t = \frac{P\ell_2^3}{3EI_2} + \frac{P\ell_1\ell_2^2}{2EI_2} + \frac{6P\ell_2}{5GA_2} + \left(\frac{P\ell_2^2}{2EI_2} + \frac{P\ell_1\ell_2}{EI_2}\right)\cdot \ell_2 + \frac{P\ell_1^3}{3EI_1} + \frac{P\ell_1}{\chi GA_1}$$

Using this expression, the total transverse displacement is equal to 0·03393″. Modelling the problem using the 3DLCS element we can reach the result equal to 0·034846″. It can be noted that the 3DLCS result is larger than the analytical solution. This is because the analytical solution assumes that the two middle surfaces coincide, which is not the case of this example.

6.2. *Rectangular plate examples*

It is well known that all the single layer theories (FSDT, LCST, etc.) are adequate[9,20,31,32] in representing global behaviour (deflections, fundamental frequencies, etc.) but only the LCST are adequate in representing the shear distribution or other local effects (delamination, etc.). Here we want to show that the proposed element retains all the positive characteristics of the single layer theories and is also capable of predicting accurately the stress distribution.

Figure 6 shows the variation of the dimensionless centre deflection $\bar{w} = [w_c(E_2h^3)/(q_0a^4)] \times 10^3$ vs. the b/a ratio and the a/h ratio of rectangular plates subjected to uniformly distributed load. The plates are made in material III and are composed by two (0°/90°) or four (0°/90°/0°/90°)

Table III. Comparison between analytical and 3DLCS solutions

Point A:	$w_b = 0{\cdot}01725''$	$w_s = 0{\cdot}00053''$	$w_t = 0.01778''$	$w_{3DLCS} = 0{\cdot}01750''$
Point B:	$w_b = 0{\cdot}00538''$	$w_s = 0{\cdot}00026''$	$w_t = 0{\cdot}00565''$	$w_{3DLCS} = 0{\cdot}00552''$

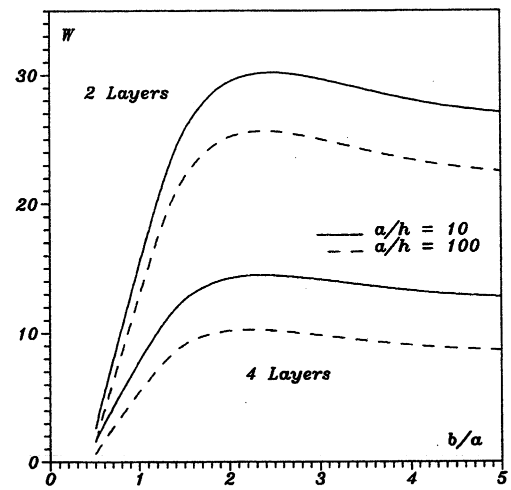

Figure 6. Centre deflections vs. b/a ratio and a/h ratio for a rectangular cross-ply plate under uniform transverse load

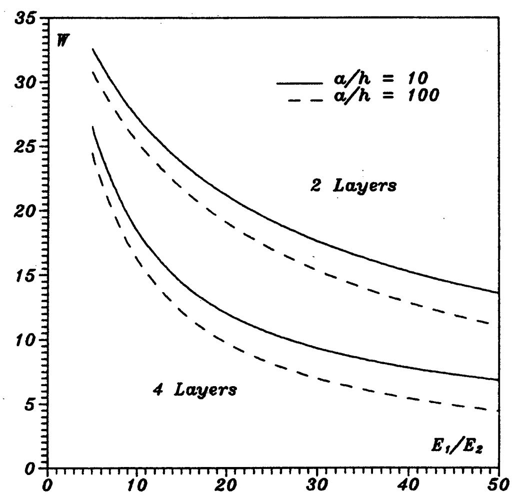

Figure 7. Effect of material anisotropy on the dimensionless centre deflections of cross-ply laminates under a uniform transverse load for different a/h ratios

layers and are subjected to SS boundary conditions. A mesh of $3 \times 3 \times$ (number of layers) was used to discretize the structures.

Comparing the results obtained using two layers with those analogous of four layers it should be observed that the influence of coupling may be extremely relevant. The centre deflection, in fact, rapidly reaches the uncoupled solution as the number of layer increases.[33] Furthermore, when the b/a ratio increases, the dimensionless centre transverse deflection becomes asymptotic, with different values for each laminate.

Figure 7 plots the non-dimensional transverse centre deflection $\bar{w} = w_c[(E_2h^3)/(q_0a^4)] \times 10^3$ versus the E_1/E_2 ratio of simply supported (SS) cross-ply plate made with two or four layers. The material is the same as material III, except for the value of E_1, varying with the ratio E_1/E_2. A mesh of $3 \times 3 \times$(number of layers) was used and a uniformly transverse distributed load was applied on the top surface of the plate. The influence of the shear deformability on the bending is shown, in the same figure, by the comparison between results relative to both ratios $a/h = 100$ and $a/h = 10$. In particular the Classical Plate Theory (simulated by $a/h = 100$) underpredicts deflections, while when the number of layers increases the solution tends to the uncoupled solution.

A moderately thick simply-supported (SS) square $(\ell \cdot \ell)$ plate made by four laminae $(45°/-45°/45°/-45°)$ was analysed to compare the shear stress distribution through the thickness, obtained using both equilibrium and constitutive equations. The layers are made by material III and a mesh of $4 \times 4 \times 4$ 3DLCS elements was used to discretize all the structure. The stress $\sigma_{x'z'}$ is calculated at the point $(\ell/2, 0)$ and the stress $\sigma_{y'z'}$ at the point $(0, \ell/2)$ by extrapolating to the nodes the stress values calculated at the reduced Gauss points.[27] The stresses are adimensionalised by the relation $\bar{\sigma}_i = [(\sigma_i h)/(q\ell)] \times 10$ $(i = x'z', y'z')$. The difference between the results, shown in Figure 8, is very clear and the excellent representation of the shear stresses obtained using the equilibrium equations is demonstrated.

To compare the results obtained using the exact three-dimensional solution of Pagano[34,35] and the analogous one determined using the proposed element, a simply supported (SS), square $(\ell \cdot \ell)$ cross-ply $(0°/90°/0°)$ plate under sinusoidal distributed load $(q = q_0 \cos[(\pi x)/\ell] \cos[(\pi y)/\ell])$ was analysed. The material adopted is material II. Owing to the symmetry, only a quarter of the plate was modelled by a $4 \times 4 \times 3$ mesh of 3DLCS elements (see Figure 9). The shear stresses are computed at the same points of the previous example, while the relation for the

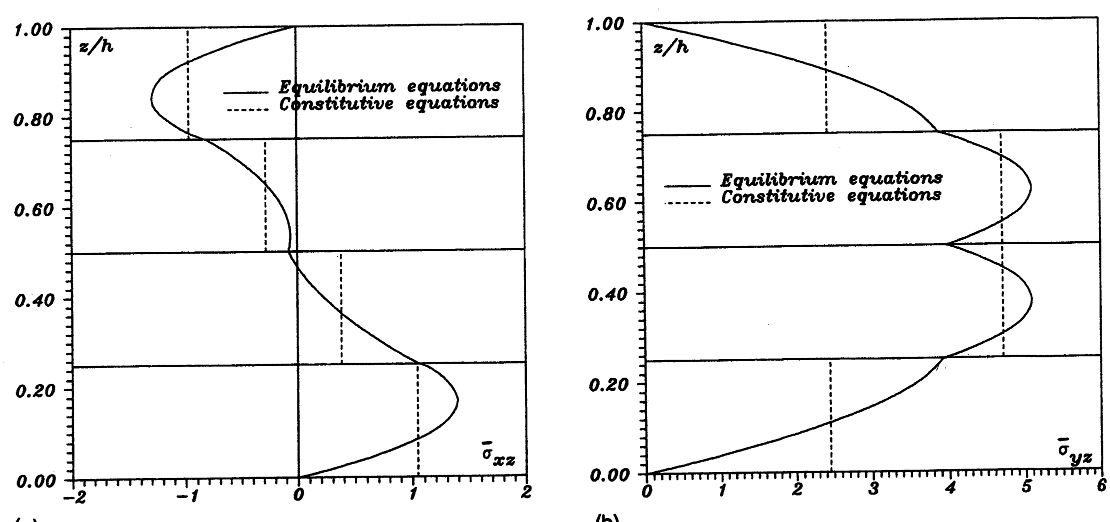

Figure 8. Square angle-ply plate under uniform transverse distributed load. Shear stresses distributions obtained using the constitutive and the equilibrium equations

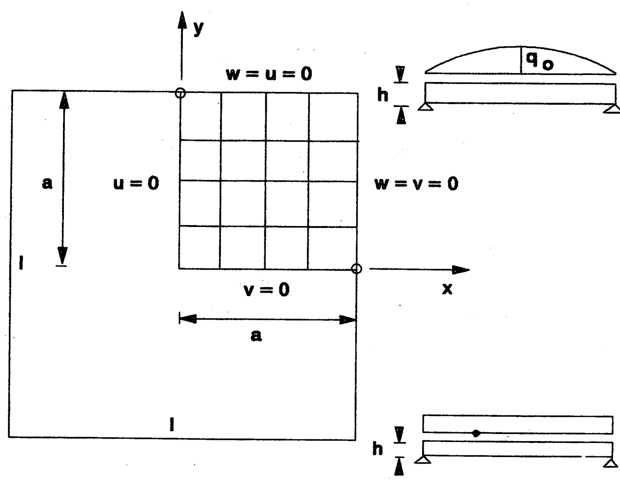

Figure 9. Scheme adopted for the calculation of the shear stresses

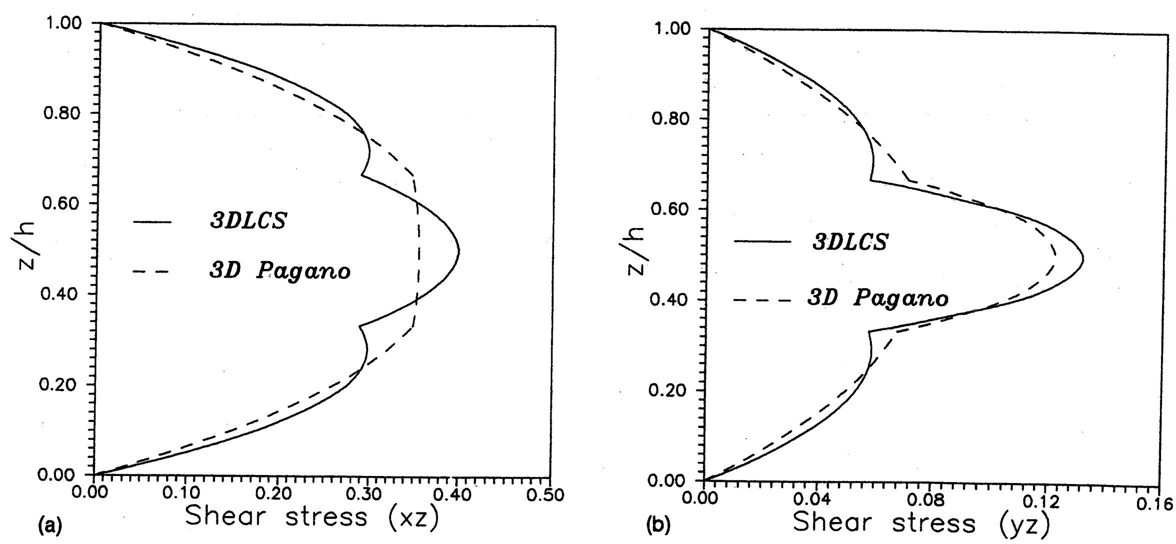

Figure 10. Shear stress distributions. Comparison between the three-dimensional exact solution of Pagano[34,35] and the 3DLCS solution

adimensionalized values is $\bar{\sigma}_i = (\sigma_i h)/(q\ell)$. Observing the plots reported in Figure 10 we can say that the results compare well, especially for $\sigma_{y'z'}$.

6.3. *Doubly curved shells*

Simply supported (SS) doubly curved shells subjected to point load (case 1) and clamped doubly curved shells under uniformly transverse (case 2) load are analysed to show the results making comparisons with the analogous results obtained running the commercial program NISA II. The structures are made in material I (isotropic). The scheme of the structures, the

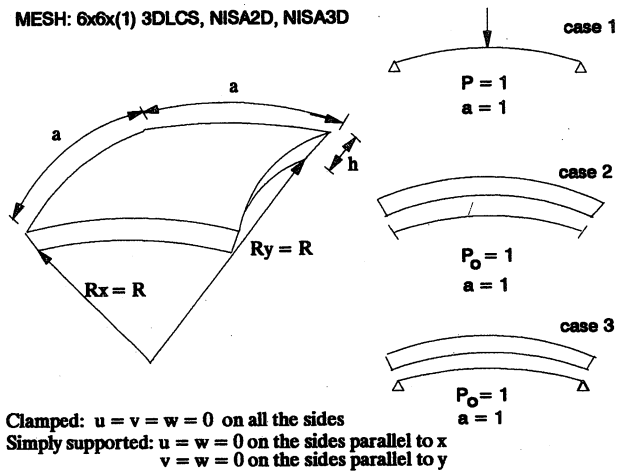

Figure 11. Schemes adopted for the calculation of the central deflections of doubly curved shells

Table IV. Central deflections of doubly curved isotropic shells vs. R/a ratio: simply supported (SS), unit point load, $a/h = 100$; exact solution for plate (CPT): $w_{max} = 0.01159$ $(Pa^2)/D = 4{\cdot}3813269$, $D = (Eh^3)/12(1-\nu^2)$)

R/a	NISA 3D	NISA 2D	3DLCS
1	5·78166E − 2	1·40893E − 1	1·45710E − 1
2	1·51658E − 1	2·78430E − 1	2·86300E − 1
3	2·63578E − 1	4·16383E − 1	4·28300E − 1
4	3·85492E − 1	5·55650E − 1	5·70400E − 1
5	5·12533E − 1	6·98147E − 1	7·14650E − 1
10	1·15077	1·46923	1·47520
Plate	4·06331	4·36106	4·39190

Table V. Central deflections of doubly curved isotropic shells vs. R/a ratio: simply supported (SS), unit point load, $a/h = 10$

R/a	NISA 3D	NISA 2D	3DLCS
1	1·99103E − 3	1·98043E − 3	2·25820E − 3
2	3·12546E − 3	3·37294E − 3	3·56840E − 3
3	3·84640E − 3	4·15647E − 3	4·29650E − 3
4	4·25647E − 3	4·57206E − 3	4·68010E − 3
5	4·49418E − 3	4·80441E − 3	4·89570E − 3
10	4·87014E − 3	4·94077E − 3	5·23420E − 3
Plate	5·01545E − 3	5·05799E − 3	5·4028E − 3

Table VI. Central deflections of doubly curved isotropic shells vs. R/a ratio: clamped (CC), unit uniformly distributed load, $a/h = 100$; exact solution for plate (CPT): $w_{max} = 0{\cdot}00126(P_0a^4)/D = 0{\cdot}4763133$, $D = (Eh^3)/12(1 - \nu^2)$)

R/a	NISA 3D	NISA 2D	3DLCS
1	1·58882E − 3	1·44643E − 3	1·44760E − 3
2	8·24728E − 3	6·67833E − 3	6·65190E − 3
3	2·08598E − 2	1·74369E − 2	1·72450E − 2
4	3·80322E − 2	3·34819E − 2	3·30970E − 2
5	5·81030E − 2	5·33332E − 2	5·28820E − 1
10	1·62102E − 1	1·70116E − 1	1·70910E − 1
Plate	3·68658E − 1	4·57171E − 1	4·80066E − 1

Table VII. Central deflections of doubly curved isotropic shells vs. R/a ratio: clamped (CC), unit uniformly distributed load, $a/h = 10$

R/a	NISA 3D	NISA 2D	3DLCS
1	1·68276E − 4	1·59774E − 4	1·59690E − 4
2	3·44046E − 4	3·54020E − 4	3·54200E − 4
3	4·21006E − 4	4·46281E − 4	4·46600E − 4
4	4·56534E − 4	4·90600E − 4	4·91020E − 4
5	4·75061E − 4	5·14460E − 4	5·14890E − 4
10	5·02076E − 4	5·51391E − 4	5·51330E − 4
Plate	5·13700E − 4	5·68437E − 4	5·68960E − 4

Table VIII. Central deflections of doubly curved laminated composite shells vs. R/a ratio simply supported (SS) (0°/90°/0°), unit uniformly distributed load

	$a/h = 10$		$a/h = 100$	
R/a	NISA 2D Composite	3DLCS	NISA 2D Composite	3DLCS
1	3·06719E − 6	2·30320E − 6	4·06942E − 5	3·84510E − 5
2	5·86618E − 6	5·72680E − 6	1·76640E − 4	1·74770E − 4
3	7·34053E − 6	7·42870E − 6	4·04504E − 4	4·00060E − 4
4	8·02942E − 6	8·27830E − 6	7·10676E − 4	7·02570E − 4
5	8·39443E − 6	8·74980E − 6	1·07565E − 3	1·06210E − 3
10	8·95673E − 6	9·52870E − 6	3·12796E − 3	3·09750E − 3
Plate	9·21828E − 6	9·98320E − 6	7·74179E − 3	7·76380E − 3

Plate under sinusoidal load: $a/h = 100$: Pagano: 0·49630E-3; 3DLCS: 0·49673E-3
$a/h = 10$: Pagano: 6·25400E-6; 3DLCS: 6·4440E-6

boundary conditions and the loads are reported in Figure 11. The results are reported in Tables from IV to VII for various R/a ratios and for two ratios of a/h.

The elements used in NISA II[28] are individuated in its library by the parameters NISA 3D: brick elements with 20 nodes, NKTP = 4, NORDR = 2 and NISA 2D: two-dimensional thick and thin shell element with 8 nodes, NKTP = 20, NORDR = 20.

When the two-dimensional mesh is adopted the simply supported boundary conditions (SS) are: $u = w = \psi_x = 0$ on all the sides parallel to the x-axis and $v = w = \psi_y = 0$ on all the sides parallel to the y-axis; ψ_x and ψ_y being the rotation along x- and y-axis, respectively. For the plate cases the exact solution of the Classical Plate Theory is reported[36] and is clear that the 3DLCS solution is the nearest solution when the structure is thin and the CPT is valid. Note that, when the shell is thin the solution obtained using the brick elements of NISA is very different from the other two solutions.

These denotes the well known effect of the ill-conditioned equations discussed by Ahmad *et al.*[18] due to the ε_z different from zero. The 3DLCS element, instead, is a solid element but the condition that ε_z is omitted in the equations (6), (9) and (23), overcomes this problem. When the structure became thick the three solutions are not very different. The 3DLCS element shows that it is more deformable taking the shear effects into better account. Also the 3DLCS solution is less expensive than the 3-D continuum elements.

Finally, doubly curved cross-ply (0°/90°/0°) shells under SS boundary conditions and uniformly transverse distributed load (case 3), are analysed. Each layer is made in material II, the mesh adopted is $4 \times 4 \times 3$ on all the structures. Two-dimensional shell elements for the analysis of laminated composite structures of the commercial program NISA II are used to model the same example using a 4×4 mesh of eight nodes elements (NKTP = 32, NORDR = 2). For the two-dimensional case the same boundary conditions (SS) of the previous case were adopted.

The comparisons are reported in Table VIII for $a/h = 10$ and $a/h = 100$ and for various R/a ratios. It is easy to note the good agreement between the results, demonstrating the capability of the 3DLCS elements to model composite laminated shell-type structures. In the plate case it is clear that the proposed element takes better account of the shear deformability. For this case the comparison with the three-dimensional exact solution of Pagano, for a sinusoidal distributed transverse load, is also reported, showing good agreement with the 3DLCS solution. For the smaller R/a ratios the use of the proposed element takes better account of the influence of the boundary conditions. In fact, in the two-dimensional model the boundary conditions are on the boundary of the middle surface and rotations around this boundary is possible. The effect is more evident for small values of the ratio R/a.

7. CONCLUSIONS

In this paper a continuum-based implementation of layer-wise constant shear theories for general laminated composite shell-type structure was presented. After the analysis of the single-layer theories, the LCST, and the 3-D continuum elements, all the positive and negative characteristics of these formulations were pointed out. Thus, a new 3DLCS element was proposed to retain only the positive characteristics of the previous analysis and to avoid the problems of the ill-conditioned equations of the 3-D continuum elements, the non precise calculation of the stress distribution of the single-layer theories, and the large number of d.o.f per node, stress resultants, and boundary conditions of the two-dimensional LCST. The proposed element has smaller number of d.o.f and the interpretation of the d.o.f, the stress resultants and the boundary conditions is intuitive as in the 3-D continuum elements. The element is capable of modelling problems with variable number of layers and thicknesses. The accuracy of the 3DLCS element was demonstrated by standard examples used to evaluate the mechanical behaviour of beams, plates and shells.

ACKNOWLEDGEMENTS

The first author would like to express his sincere gratitude to his advisors, Profs. Domenico Bruno and Giuseppe Spadea, for their encouragement to develop the present work. The constructive discussions and suggestions of Roberto Lopez–Anido are also acknowledged. The second author acknowledges partial support from NATO Grant CRG 910943.

APPENDIX I

List of symbols

x, y, z	global co-ordinates
x', y', z'	surface co-ordinates
1, 2, 3	lamina material directions (1 = fibre direction)
ξ, η, ζ	elemental co-ordinates
N_i	interpolations functions in global co-ordinates
$\{\mathbf{u}\}, \{\mathbf{u}'\}$	displacement vector in global and surface co-ordinates, respectively
$\{\boldsymbol{\delta}_i\}$	nodal displacement vector
$\{\boldsymbol{\delta}^e\}$	elemental displacement vector
$\mathcal{N}$	number of nodes in the mesh
$\{\boldsymbol{\sigma}\}; \{\boldsymbol{\sigma}'\}$	stress vectors in global and surface co-ordinates, respectively
$\{\boldsymbol{\varepsilon}\}; \{\boldsymbol{\varepsilon}'\}$	strain vectors in global and surface co-ordinates, respectively
$[C_{ij}]$	three-dimensional stiffness matrix
$[Q_{ij}]$	two-dimensional stiffness matrix
$[D_{ij}]$	3DLCS stiffness matrix
k	shear correction factor
E_1, E_2, E_3	Young's moduli in direction 1, 2 and 3, respectively
G_{12}, G_{13}, G_{23}	shear moduli
$\nu_{12}, \nu_{13}, \nu_{23}$	Poisson coefficients
$[\mathbf{T}^k]$	rotation matrix for the generic lamina k
$\{\mathbf{p}\}$	body forces per unit volume
$\{\mathbf{q}\}$	applied surface tractions
$[\mathbf{B}], [\mathbf{B}']$	strain–displacement matrices in global and surface co-ordinates, respectively
$[\mathbf{K}]$	shell stiffness matrix in global co-ordinates
$\{\mathbf{F}\}$	equivalent nodal forces
$[\mathbf{J}]$	Jacobian matrix
$\{\mathbf{V}_1\}, \{\mathbf{V}_2\}, \{\mathbf{V}_3\}$	vectors in direction x', y' and z', respectively
$\{\mathbf{i}\}, \{\mathbf{j}\}, \{\mathbf{k}\}$	unit vectors in direction x, y and z, respectively
$\{\mathbf{v}_1\}, \{\mathbf{v}_2\}, \{\mathbf{v}_3\}$	unit vectors in direction x', y' and z', respectively
$[\boldsymbol{\Theta}]$	matrix of unit vectors in x', y' and z' direction (rotation matrix)
$\nabla\nabla N, \nabla\nabla N'$	gradient of the gradient of each interpolation function in global and surface co-ordinates, respectively
$[\mathbf{B}'_{x'}], [\mathbf{B}'_{y'}]$	matrices of second derivatives of interpolation functions respect x' and y' co-ordinate, respectively

P_i component of the distributed load in direction i
A area of upper, middle or bottom surface of the 3DLCS element, depending on the position of the loading
T_H thickness of the 3DLCS element at each Gaussian point
W weight at each Gaussian point
ngp number of Gaussian points
$[\mathbf{H}]$ operator of differentials
$[\mathbf{A}]$ constraint matrix

APPENDIX II

Computation of higher-order derivatives

The computation of the second derivatives of the interpolation functions with respect to the global co-ordinates involves additional computations.

The first order derivatives with respect to the global co-ordinates are related to those with respect to the elemental co-ordinate according to

$$\begin{Bmatrix} \dfrac{\partial N_i}{\partial x} \\[2ex] \dfrac{\partial N_i}{\partial y} \\[2ex] \dfrac{\partial N_i}{\partial z} \end{Bmatrix} = \begin{bmatrix} \dfrac{\partial x}{\partial \xi} & \dfrac{\partial y}{\partial \xi} & \dfrac{\partial z}{\partial \xi} \\[2ex] \dfrac{\partial x}{\partial \eta} & \dfrac{\partial y}{\partial \eta} & \dfrac{\partial z}{\partial \eta} \\[2ex] \dfrac{\partial x}{\partial \zeta} & \dfrac{\partial y}{\partial \zeta} & \dfrac{\partial z}{\partial \zeta} \end{bmatrix}^{-1} \begin{Bmatrix} \dfrac{\partial N_i}{\partial \xi} \\[2ex] \dfrac{\partial N_i}{\partial \eta} \\[2ex] \dfrac{\partial N_i}{\partial \zeta} \end{Bmatrix} = [\mathbf{J}]^{-1} \begin{Bmatrix} \dfrac{\partial N_i}{\partial \xi} \\[2ex] \dfrac{\partial N_i}{\partial \eta} \\[2ex] \dfrac{\partial N_i}{\partial \zeta} \end{Bmatrix} \tag{36}$$

where the Jacobian $[\mathbf{J}]$ is evaluated using the approximation of the geometry.

The second derivative of N_i with respect to the elemental co-ordinate (x, y, z) are given by

$$\begin{Bmatrix} \dfrac{\partial^2 N_i}{\partial \xi^2} \\[2ex] \dfrac{\partial^2 N_i}{\partial \eta^2} \\[2ex] \dfrac{\partial^2 N_i}{\partial \zeta^2} \\[2ex] \dfrac{\partial^2 N_i}{\partial \eta \partial \zeta} \\[2ex] \dfrac{\partial^2 N_i}{\partial \xi \partial \zeta} \\[2ex] \dfrac{\partial^2 N_i}{\partial \xi \partial \eta} \end{Bmatrix} = [\mathbf{J}^1] \begin{Bmatrix} \dfrac{\partial^2 N_i}{\partial x^2} \\[2ex] \dfrac{\partial^2 N_i}{\partial y^2} \\[2ex] \dfrac{\partial^2 N_i}{\partial z^2} \\[2ex] \dfrac{\partial^2 N_i}{\partial y \partial z} \\[2ex] \dfrac{\partial^2 N_i}{\partial x \partial z} \\[2ex] \dfrac{\partial^2 N_i}{\partial x \partial y} \end{Bmatrix} + [\mathbf{J}^2] \begin{Bmatrix} \dfrac{\partial N_i}{\partial x} \\[2ex] \dfrac{\partial N_i}{\partial y} \\[2ex] \dfrac{\partial N_i}{\partial z} \end{Bmatrix} \tag{37}$$

Then the second derivative respect to the global co-ordinate are given by

$$\begin{Bmatrix} \dfrac{\partial^2 N_i}{\partial x^2} \\ \dfrac{\partial^2 N_i}{\partial y^2} \\ \dfrac{\partial^2 N_i}{\partial z^2} \\ \dfrac{\partial^2 N_i}{\partial y \partial z} \\ \dfrac{\partial^2 N_i}{\partial x \partial z} \\ \dfrac{\partial^2 N_i}{\partial x \partial y} \end{Bmatrix} = [\mathbf{J}^1]^{-1} \left[\begin{Bmatrix} \dfrac{\partial^2 N_i}{\partial \xi^2} \\ \dfrac{\partial^2 N_i}{\partial \eta^2} \\ \dfrac{\partial^2 N_i}{\partial \zeta^2} \\ \dfrac{\partial^2 N_i}{\partial \eta \partial \zeta} \\ \dfrac{\partial^2 N_i}{\partial \xi \partial \zeta} \\ \dfrac{\partial^2 N_i}{\partial \xi \partial \eta} \end{Bmatrix} - [\mathbf{J}^2] \begin{Bmatrix} \dfrac{\partial N_i}{\partial x} \\ \dfrac{\partial N_i}{\partial y} \\ \dfrac{\partial N_i}{\partial z} \end{Bmatrix} \right] \tag{38}$$

where the coefficients of $[\mathbf{J}^1]$ and $[\mathbf{J}^2]$ are the following:

$$J^1_{11} = \left(\frac{\partial x}{\partial \xi}\right)^2, \quad J^1_{12} = \left(\frac{\partial y}{\partial \xi}\right)^2, \quad J^1_{13} = \left(\frac{\partial z}{\partial \xi}\right)^2$$

$$J^1_{14} = 2\frac{\partial y}{\partial \xi}\frac{\partial z}{\partial \xi}, \quad J^1_{15} = 2\frac{\partial x}{\partial \xi}\frac{\partial z}{\partial \xi}, \quad J^1_{16} = 2\frac{\partial x}{\partial \xi}\frac{\partial y}{\partial \xi}$$

$$J^1_{21} = \left(\frac{\partial x}{\partial \eta}\right)^2, \quad J^1_{22} = \left(\frac{\partial y}{\partial \eta}\right)^2, \quad J^1_{23} = \left(\frac{\partial z}{\partial \eta}\right)^2$$

$$J^1_{24} = 2\frac{\partial y}{\partial \eta}\frac{\partial z}{\partial \eta}, \quad J^1_{25} = 2\frac{\partial x}{\partial \eta}\frac{\partial z}{\partial \eta}, \quad J^1_{26} = 2\frac{\partial x}{\partial \eta}\frac{\partial y}{\partial \eta}$$

$$J^1_{31} = \left(\frac{\partial x}{\partial \zeta}\right)^2, \quad J^1_{32} = \left(\frac{\partial y}{\partial \zeta}\right)^2, \quad J^1_{33} = \left(\frac{\partial z}{\partial \zeta}\right)^2$$

$$J^1_{34} = 2\frac{\partial y}{\partial \zeta}\frac{\partial z}{\partial \zeta}, \quad J^1_{35} = 2\frac{\partial x}{\partial \zeta}\frac{\partial z}{\partial \zeta}, \quad J^1_{36} = 2\frac{\partial x}{\partial \zeta}\frac{\partial y}{\partial \zeta}$$

$$J^1_{41} = \frac{\partial x}{\partial \eta}\frac{\partial x}{\partial \zeta}, \quad J^1_{42} = \frac{\partial y}{\partial \eta}\frac{\partial y}{\partial \zeta}, \quad J^1_{43} = \frac{\partial z}{\partial \eta}\frac{\partial z}{\partial \zeta}$$

$$J^1_{44} = \frac{\partial y}{\partial \eta}\frac{\partial z}{\partial \zeta} + \frac{\partial z}{\partial \eta}\frac{\partial y}{\partial \zeta}, \quad J^1_{45} = \frac{\partial x}{\partial \eta}\frac{\partial z}{\partial \zeta} + \frac{\partial x}{\partial \zeta}\frac{\partial z}{\partial \eta}, \quad J^1_{46} = \frac{\partial x}{\partial \eta}\frac{\partial y}{\partial \zeta} + \frac{\partial y}{\partial \eta}\frac{\partial x}{\partial \zeta}$$

$$J^1_{51} = \frac{\partial x}{\partial \xi}\frac{\partial x}{\partial \zeta}, \quad J^1_{52} = \frac{\partial y}{\partial \xi}\frac{\partial y}{\partial \zeta}, \quad J^1_{53} = \frac{\partial z}{\partial \xi}\frac{\partial z}{\partial \zeta}$$

$$J^1_{54} = \frac{\partial y}{\partial \xi}\frac{\partial z}{\partial \zeta} + \frac{\partial y}{\partial \zeta}\frac{\partial z}{\partial \xi}, \quad J^1_{55} = \frac{\partial x}{\partial \xi}\frac{\partial z}{\partial \zeta} + \frac{\partial x}{\partial \zeta}\frac{\partial z}{\partial \xi}, \quad J^1_{56} = \frac{\partial x}{\partial \xi}\frac{\partial y}{\partial \zeta} + \frac{\partial x}{\partial \zeta}\frac{\partial y}{\partial \xi}$$

$$J^1_{61} = \frac{\partial x}{\partial \xi}\frac{\partial x}{\partial \eta}, \quad J^1_{62} = \frac{\partial y}{\partial \xi}\frac{\partial y}{\partial \eta}, \quad J^1_{63} = \frac{\partial z}{\partial \xi}\frac{\partial z}{\partial \eta}$$

$$J^1_{64} = \frac{\partial y}{\partial \xi}\frac{\partial z}{\partial \eta} + \frac{\partial y}{\partial \eta}\frac{\partial z}{\partial \xi}, \quad J^1_{65} = \frac{\partial x}{\partial \xi}\frac{\partial z}{\partial \eta} + \frac{\partial x}{\partial \eta}\frac{\partial z}{\partial \xi}, \quad J^1_{66} = \frac{\partial x}{\partial \xi}\frac{\partial y}{\partial \eta} + \frac{\partial x}{\partial \eta}\frac{\partial y}{\partial \xi}$$

$$J^2_{11} = \frac{\partial^2 x}{\partial \xi^2}, \quad J^2_{12} = \frac{\partial^2 y}{\partial \xi^2}, \quad J^2_{13} = \frac{\partial^2 z}{\partial \xi^2}$$

$$J^2_{21} = \frac{\partial^2 x}{\partial \eta^2}, \quad J^2_{22} = \frac{\partial^2 y}{\partial \eta^2}, \quad J^2_{23} = \frac{\partial^2 z}{\partial \eta^2}$$

$$J^2_{31} = \frac{\partial^2 x}{\partial \zeta^2}, \quad J^2_{32} = \frac{\partial^2 y}{\partial \zeta^2}, \quad J^2_{33} = \frac{\partial^2 z}{\partial \zeta^2}$$

$$J^2_{41} = \frac{\partial^2 x}{\partial \eta \partial \zeta}, \quad J^2_{42} = \frac{\partial^2 y}{\partial \eta \partial \zeta}, \quad J^2_{43} = \frac{\partial^2 z}{\partial \eta \partial \zeta}$$

$$J^2_{51} = \frac{\partial^2 x}{\partial \xi \partial \zeta}, \quad J^2_{52} = \frac{\partial^2 y}{\partial \xi \partial \zeta}, \quad J^2_{53} = \frac{\partial^2 z}{\partial \xi \partial \zeta}$$

$$J^2_{61} = \frac{\partial^2 x}{\partial \xi \partial \eta}, \quad J^2_{62} = \frac{\partial^2 y}{\partial \xi \partial \eta}, \quad J^2_{63} = \frac{\partial^2 z}{\partial \xi \partial \eta}$$

REFERENCES

1. S. A. Ambartsumyan, *Theory of Anisotropic Shells*, Moscow, 1961, English translation, NASA TT F-118, Dover, San Francisco, CA 1964.
2. S. B. Dong and R. L. Taylor, 'On the theory of laminated anisotropic shells and plates', *J. Aerospace Sci.*, **29**, 969–975 (1962).
3. W. T. Koiter, 'A consistent first approximation in the general theory of thin elastic shells, accurate and simple fourth order governing equations', *Proc. Symp. Theory of Thin Elastic Shells*, North-Holland, Amsterdam 1960, pp. 12–13.
4. J. N. Reddy, 'Exact solutions of moderately thick laminated shells', *J. Eng. Mech. Div.* ASCE, **110**, 794 (1984).
5. J. N. Reddy and K. Chandrashekhara, 'Geometrically non-linear transient analysis of laminated, doubly-curved shells', *Int. J. Non-Linear Mech.*, **20**(2), 79–90 (1985).
6. D. Bruno, S. Lato and R. Zinno, 'Non linear analysis of doubly-curved composite shells', *Comp. Eng.*, **3**, 419–435 (1993).
7. J. N. Reddy, 'On the generalization of displacement-based laminate theories', *Appl. Mech. Rev.*, **42,** S213–s222 (1989).
8. J. N. Reddy, 'A generalization of two dimensional theories of laminated plates', *Commun. appl. numer. methods*, **3,** 113–180 (1987).
9. E. J. Barbero, 'On a generalized laminate plate theory with application to bending, vibration and delamination buckling in composite laminates', *Ph.D. Dissertation*, Virginia Polytechnic Institute, Blacksburg, VA, 1989.
10. E. J. Barbero, J. N. Reddy and J. L. Teply, 'General two-dimensional theory of laminated cylindrical shells', *AIAA J.*, **28,** 544–553 (1990).
11. S. Srinivas, 'Refined analysis of composite laminates', *J. Sound Vib.*, **30,** 495–507 (1973).
12. P. Seide, 'An improved approximate theory for the bending of laminated plates', *Mech. Today*, **5,** 451–456 (1980).
13. M. Epstein and P. G. Glockner, 'Non linear analysis of multilayered shells', *Int. J. Solids Struct.*, **13,** 1081–1089 (1977).
14. M. Epstein and H. P. Huttelmajer, 'A finite element formulation for multilayered and thick plates', *Comput. Struct.*, **16,** 645–650 (1983).
15. M. Murakami, 'Laminated composite plate theories with improved inplane responses', *Proc. ASME Pressure Vessels and Piping Conf.*, 1984, pp. 257–263.
16. R. L. Hinrichsen and A. N. Palazzotto, 'The nonlinear finite element analysis of thick composite plates using a cubic spline function', *AIAA J.*, **24,** 1836–1842 (1986).
17. D. R. J. Owen and Z. H. Li, 'A refined analysis of laminated plates by finite element displacement methods, I Fundamentals and static analysis; II vibrations and stability', *Comput. Struct.*, **26,** 907–923 (1987).
18. S. Ahmad, B. M. Irons and O. C. Zienkiewicz, 'Analysis of thick and thin shell structures by curved finite elements', *Int. j. numer. methods eng.*, **2,** 419–451 (1970).
19. E. J. Barbero, '3-D Finite element modeling of laminated composites by layer-wise constant shear elements', *En. An. Tech. Comp. Mat., ASME*, **10,** NDE 229–237 (1991).
20. E. J. Barbero, 'A 3-D finite element for laminated composites with a 2-D kinematic constraints', *Comput. Struct.*, **45, 263–271** (1992).
21. E. J. Barbero and R. Zinno, 'Analysis of laminated composite plates with three-dimensional layer-wise constant shear elements', *Int. J. Eng. Anal. Des.*, 1993, in press.

22. E. J. Barbero and J. N. Reddy, 'An accurate determination of stresses in thick laminates using a generalized plate theory', *Int. j. numer. methods eng.*, **29**, 1–14 (1990).
23. R. A. Chaudhuri, 'An equilibrium method for the prediction of transverse shear stresses in a thick laminated plate', *Comput. Struct.*, **23**, 139–146 (1986).
24. R. M. Jones, *Mechanics of Composite Materials*, Hemisphere Publishing Corp., New York 1975.
25. R. Zinno and E. J. Barbero, 'General anisotropic shell-type structures analysed by a 3-D layer-wise constant shear element', *CFC Report No 93/156*, June 1993, Constructed Facilities Center, West Virginia University, Morgantown, WV, USA.
26. E. J. Barbero, J. N. Reddy and J. L. Teply, 'A plate bending element, based on the generalized laminate theory: Implementation into ABAQUS computer program', *CCSM-89-08*, Virginia Polytechnic Institute and State University, Blacksburg, VA (1988).
27. R. D. Cook, *Concepts and Applications of Finite Element Analysis*, 2nd Ed. Wiley, New York 1974.
28. NISA II Version 90.0 and DISPLAY III, *Pre- & Post-Processing program Version 91.0 User's Manuals*, Eng. Mech. Res. Corp. (1990–1991).
29. R. C. Averil, 'On the nonlinear behaviour of shear deformable plate elements', *Thesis*, Virginia Polithecnic Institute and State University, Blacksburg, VA, 1989.
30. S. A. Ramaseshan, 'A linear 3-D finite element for laminated composites with layer-wise constant shear', *Master Thesis*, College of Engineering, West Virginia University, Morgantown, WV 26506, 1991.
31. J. N. Reddy, E. J. Barbero and J. L. Teply, 'A plate bending element based on a generalized laminate plate theory', *Int. j. numer. methods eng.*, **28**, 2275–2292, (1989).
32. E. J. Barbero, J. N. Reddy and J. L. Teply, 'An accurate determination of stresses in laminated plates', *Int. j. numer. methods eng.*, **29**, 1–14 (1990).
33. G. Porco, G. Spadea and R. Zinno, 'A geometrically nonlinear analysis of laminated composite plates using a shear deformation theory', *Atti Acc. dei Lincei* (*Italy*), *Rend. Fis.* (8), **LXXXIII**, 159, 176 (1989).
34. N. J. Pagano, 'Exact solutions for composite laminates in cylindrical bending', *J. Comp. Mater.*, **3**, 398–411 (1969).
35. N. J. Pagano, 'Exact solutions for rectangular bidirectional composites and sandwich plates, *J. Comp. Mater.*, **4**, 20–35 (1970).
36. A. C. Ugural, *Stresses in Plates and Shells*, McGraw-Hill New York, 1988.